Reversible multilayered vesicle-like structures with fluid hydrophobic and interpolyelectrolyte layers

Anastasiia Murmiliuk,[†] Sergey K. Filippov,[‡,⊥] Oleg Rud,[†] Peter Košovan,[†] Zdeněk Tošner,[†] Aurel Radulescu,[¶] Athanasios Skandalis,[§] Stergios Pispas,[§] Miroslav Šlouf,[‖] and Miroslav Štěpánek*[,†]

†*Department of Physical and Macromolecular Chemistry, Faculty of Science, Charles University, Hlavova 8, 128 00 Prague 2, Czech Republic*

‡ *Pharmaceutical Sciences Laboratory, Faculty of Science and Engineering, Åbo Akademi University, 20520 Turku, Finland*

¶*Forschungszentrum Jülich GmbH, Jülich Centre for Neutron Science@MLZ, Lichtenbergstraße 1, D-85747 Garching, Germany*

§ *Theoretical and Physical Chemistry Institute, National Hellenic Research Foundation, 48 Vassileos Constantinou Avenue, 11635 Athens, Greece*

‖*Institute of Macromolecular Chemistry, Czech Academy of Sciences, Heyrovského náměstí 2, Prague 6, 162 06, Czech Republic*

⊥ *Department of Chemistry and Chemical Technology, Al-Farabi Kazakh National University, 050040 Almaty, Kazakhstan*

E-mail: stepanek@natur.cuni.cz

Abstract

Hydrophobic blocks of amphiphilic block copolymers often form glassy micellar

cores at room temperature with a rigid structure that limits their applications as nanocapsules for targeted delivery. Nevertheless, we prepared and analyzed core/shell micelles with a soft core, formed by a self-assembled block copolymer consisting of a hydrophobic block and a polycation block, poly(lauryl acrylate)-*block*-poly(trimethylaminoethyl acrylate) (PLA-QPDMAEA), in aqueous solution. By light and small-angle neutron scattering, by transmission electron microscopy and by fluorescence spectroscopy, we showed that these core/shell micelles are spherical and cylindrical with a fluid-like PLA core and a positively charged outer shell and that they can encapsulate and release hydrophobic solutes. Moreover, after mixing these PLA-QPDMAEA core/shell micelles with another diblock copolymer, consisting of a hydrophilic block and a polyanion block, namely poly(ethylene oxide)-*block*-poly(methacrylic acid) (PEO-PMAA), we observed the formation of novel vesicle-like multicompartment structures containing both soft hydrophobic and interpolyelectrolyte (IPEC) layers. By combining small-angle neutron scattering with self-consistent field modeling, we confirmed the formation of these complex vesicle-like structures with a swollen PEO core, an IPEC inner layer, a PLA soft layer, an IPEC outer layer and a loose PEO corona. Thus, these multicompartment micelles with fluid and IPEC layers and a hydrophilic corona may be used as nanocapsules with several tunable properties, including the ability to control the thickness of each layer, the charge of the IPEC layers and the stability of the micelles, to deliver both hydrophobic and multivalent solutes.

Introduction

Nanomaterials for targeted delivery and controlled release of low-molar mass compounds must be biocompatible, biodegradable and stimuli-responsive.[1] More specifically, the stimuli-responsiveness ensures that the nanomaterial can not only encapsulate its low-molecular cargo but also release it in a specific location, or under specific conditions. The rational design of such nanomaterials requires understanding the basic principles of the complex relations between their morphology, structure and loading or release properties. Polymeric

nanocarriers formed by homopolymers, block copolymers or surfactants can be dynamically formed (and disassembled), self- or co-assembled in aqueous solutions into various structures (core/shell[2–4] or worm-like micelles,[5] lamellae[6] and vesicles,[7,8] among others), thereby efficiently encapsulating low-molar mass species.[9]

An approach to designing nanocapsules is based on the self-assembly of amphiphilic block copolymers consisting of hydrophobic and hydrophilic blocks[10–12] in aqueous solution into core/shell micelles with a core formed by the hydrophobic blocks and a shell formed by the hydrophilic blocks.[13] The morphology of such micelles depends on the ratio of the hydrophobic-to-hydrophilic block length; hydrophobic block aggregation is the driving force of the self-assembly process, whereas steric repulsion among hydrophilic blocks or electrostatic repulsion among polyelectrolyte blocks in the outer shell stops the aggregation, thus yielding aggregates of a well-defined size.[14–17] However, hydrophobic blocks of the most common amphiphilic block copolymers form core/shell micelles with a compact solid-like core at room temperature, which prevents the re-structuring of these micelles upon the action of an external stimulus, thereby limiting their prospective applications. In contrast, soft or fluid cores allow an efficient encapsulation of hydrophobic solutes into dynamic micelles. For example, some poly(n-alkyl acrylates) with a low glass transition temperature, T_g, form a soft core, whose density is determined by their self-assembly behavior.[18,19] The brush-like structure of the poly(n-alkyl acrylate) block prevents the solidification of the core, which thus forms a fluid-like and disordered structure due to the long and flexible side chains.[18,20]

Another approach to creating dynamical micelles is to co-assemble a copolymer consisting of a neutral hydrophilic block and a polyelectrolyte block with an oppositely charged polyelectrolyte[21–24] into the core/shell nanoparticles with a core formed by the insoluble interpolyelectrolyte complex (IPEC) and a shell composed of the neutral hydrophilic block. In our previous study,[25] we have shown that a block copolymer composed of a polycationic block and a neutral hydrophilic block can form core/shell micelles with an IPEC core by co-assembly with a polyanion. Using isothermal titration calorimetry and fluorescence spec-

troscopy, we demonstrated that the IPEC core remains dynamic because the chains can rearrange, even after the complex is formed.

In the present study, we combined both approaches for designing dynamical micelles with a soft core and an IPEC layer to simultaneously encapsulate both hydrophobic and multivalent compounds. We investigated the self-assembly of a novel copolymer poly(lauryl acrylate)-*block*-poly(trimethylammonioethyl acrylate) (PLA-QPDMAEA) consisting of a hydrophobic PLA block and a positively charged QPDMAEA block and its co-assembly with an oppositely charged diblock copolymer consisting of a polyanion block and a neutral hydrophilic block, namely poly(ethylene oxide)-*block*-poly(methacrylic acid) (PEO-PMAA) (Fig. 1). The PLA block is expected to form a fluid-like core, similarly to other n-alkyl acrylates, because of its high hydrophobicity and relatively low T_g of 255 K,[26] while QPDMAEA and PMAA blocks are expected to form interpolyelectrolyte complexes thanks to the presence of oppositely charged groups; since PMAA is a weak polyelectrolyte, it can be used for designing pH sensitive materials with controllable charge. All blocks of these copolymers (PLA, PDMAEA, PEO and PMAA) are biocompatible polymers and have potential applications in nanomedicine, for instance for targeted drug and gene delivery.[27,28] The authors of a recent study of a similar system composed of PLA-QPDMAEA and PAA-PEO using both experimental and simulation techniques have suggested the formation of onion-type micelles with an IPEC middle-layer between the hydrophobic core and the neutral hydrophilic corona.[29] In the current study, we combined scattering, microscopy, calorimetry and nuclear magnetic resonance with self-consistent field modeling to conduct a detailed characterization of the morphology of the IPEC complex of an amphiphilic block (PLA-QPDMAEA) with a double hydrophilic block copolymer (PEO-PMAA) in a basic aqueous solution (pH 9.2) towards understanding the physicochemical mechanisms controlling the assembly of multicompartment nanoparticles.

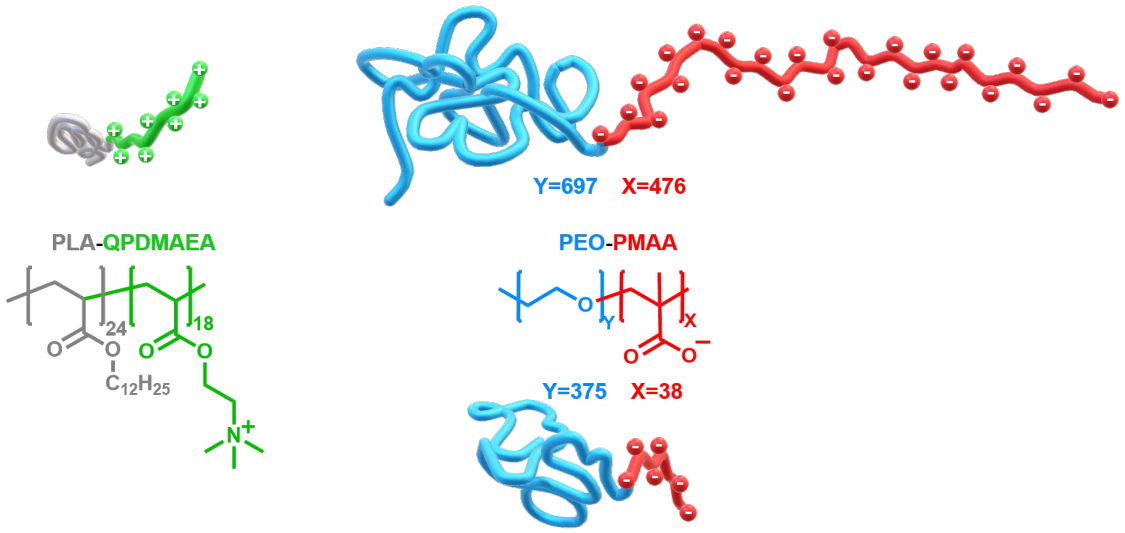

Figure 1: Chemical structures and schematic representation of PLA-QPDMAEA (left) and 'long' (top right) and 'short' (bottom right) PEO-PMAA.

Results and Discussion

Self-assembly of the amphiphilic PLA-QPDMAEA copolymer

First, we studied the solution behavior of a novel PLA-QPDMAEA copolymer; the combination of PLA and polyelectrolyte blocks allows PLA-QDMAEA to self-assemble into core/shell micelles, to encapsulate hydrophobic species and to co-assemble with oppositely charged polyelectrolytes. In order to follow the self-assembly behavior of the PLA-QPDMAEA diblock copolymer in 50 mM sodium tetraborate buffer (pH $\approx$ 9.2), we used light scattering techniques. Dynamic light scattering (DLS) measurements showed that, in aqueous solution, the copolymer forms particles with a hydrodynamic radius, R_{H}, of 50 nm measured at a scattering angle of 90° (see Fig. 2a insert). The highly positive zeta-potential, ζ, of the particles (+26 mV), determined by electrophoretic light scattering (ELS), confirms that positively charged QDMAEA groups are located on the surface of the particles.

More detailed information about the morphology of the particles was gathered by cryogenic transmission electron microscopy (cryo-TEM) and small-angle neutron scattering (SANS). Cryo-TEM showed that, in aqueous solution, PLA-QPDMAEA forms two types of particles

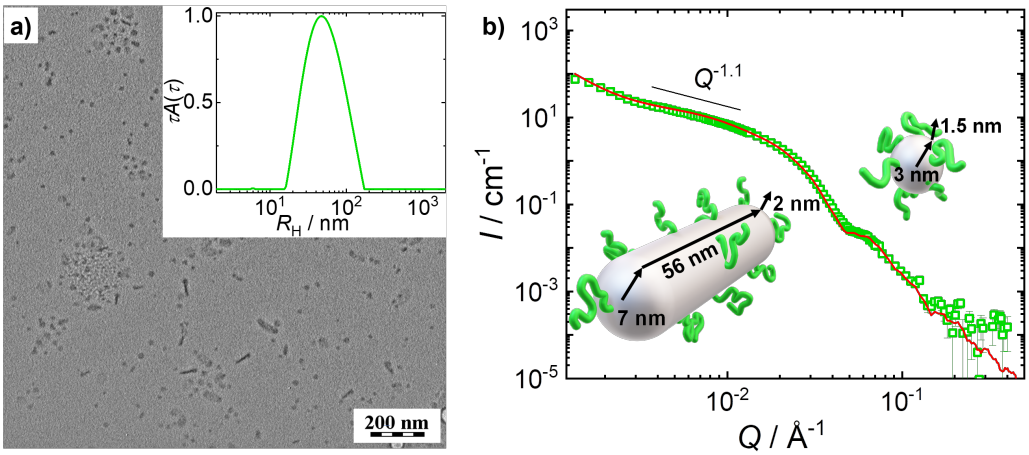

Figure 2: (a) Cryo-TEM micrograph for PLA-QPDMAEA in 50 mM sodium tetraborate. Inset: Distribution of hydrodynamic radii, R_{H}, at scattering angle $\theta = 90°$. (b) SANS curve for PLA-QPDMAEA solution; the red line is the fit of the curve using a combination of models for a randomly oriented cylindrical shell with a circular cross-section and for a sphere with a shell.

at high ionic strength (0.05 M sodium tetraborate): a large fraction of small spherical particles of $\approx$ 11 nm radius and a small fraction of cylindrical particles of $\approx$ 50 nm length and of $\approx$ 7 nm radius. This behavior is in line with the previously reported tendency of amphiphilic polyelectrolyte diblock copolymers to assemble into cylindrical particles at a high ionic strength due to the strong electrostatic screening of charged blocks.[30–33] The co-existence of spherical and cylindrical particles can be caused by high dispersity of PLA-QPDMAEA copolymer (1.41) and therefore significant differences in properties of polymers with different chain lengths.

Further insight into the structure of PLA-QPDMAEA micelles was revealed by fitting the SANS curves, as shown in Fig. 2b. In the fit, we used a linear combination of models of a randomly oriented cylindrical shell with a circular cross-section and a spherical core surrounded by a shell (see description of the models in ESI, Section S2.5.1). The fit revealed a core/shell structure of both cylindrical and spherical particles formed by PLA-QPDMAEA in aqueous solution, presumably consisting of a hydrophobic PLA core and a QPDMAEA outer shell. The dimensions of the micelles that were determined by fitting the SANS curve

match those assessed by cryo-TEM: the spherical particles have a core of 3 nm radius and 1.5 nm shell thickness, whereas the cylindrical particles have a core of 56 nm length and of 7 nm radius, and a shell of 2 nm thickness, see also Fig. 2b. The upturn at 0.003 A^{-1} indicates the presence of a negligible fraction of aggregates, that was observed in cryo-TEM micrographs as well (Fig. S8).

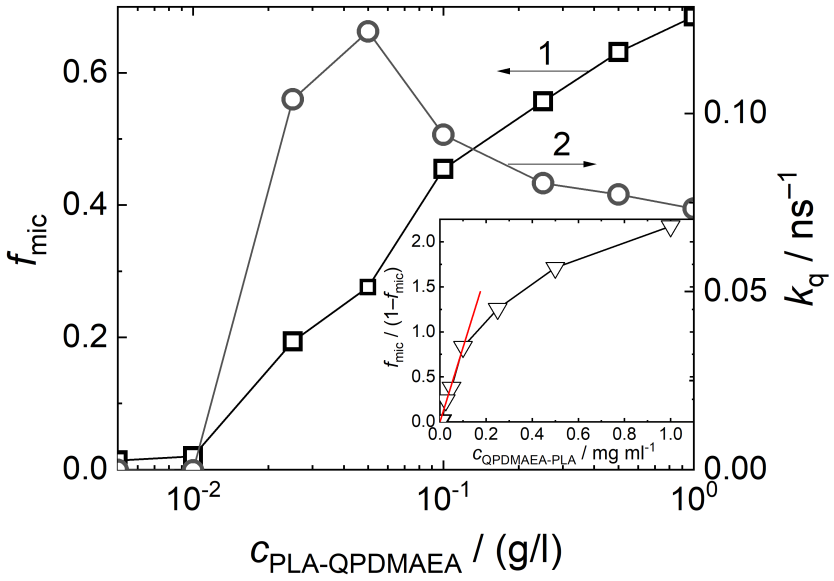

Figure 3: The fraction of integral emission intensity of pyrene in the micellar pseudophase normalized to 1, f_{mic}, and the quenching constant for pyrene in the micellar pseudophase, k_{q}, determined by fitting the fluorescence emission intensity decays of PLA-QPDMAEA solutions with pyrene to eq.1, as a function of PLA-QPDMAEA concentration, $c_{\mathrm{PLA-QPDMAEA}}$.

Having established the core/shell structure of PLA-QPDMAEA micelles, we studied the partitioning of pyrene as a hydrophobic fluorescent probe between the aqueous pseudophase and the micellar pseudophase. In PLA-QPDMAEA micelles, pyrene is efficiently quenched both by QPDMAEA segments and iodide I^- counterions and its decay can thus be described by the micellar quenching model.[34] Together with the contribution from pyrene in the aqueous pseudophase, the decay function for pyrene in PLA-QPDMAEA aqueous solutions is

$$F(t) = A_{\mathrm{mic}} \exp\Big(-t/\tau_{\mathrm{mic}} - C[1 - \exp(-k_q t)]\Big) + A_{\mathrm{aq}} \exp(-t/\tau_{\mathrm{aq}}) + B \qquad (1)$$

where A_{mic} and A_{aq} are the fractions of pyrene emission intensities for the micellar and aqueous pseudophases at $t = 0$, τ_{mic} and τ_{aq} are the lifetimes of pyrene in the micellar and aqueous pseudophases, C is the average number of quenchers per one pyrene molecule and k_{q} is the quenching constant for pyrene in the micellar pseudophase and B is the background. The fraction of integral emission intensity of pyrene in the micellar pseudophase normalized to 1 is

$$f_{\mathrm{mic}} = \frac{A_{\mathrm{mic}}\varphi_{\mathrm{mic}}}{A_{\mathrm{mic}}\varphi_{\mathrm{mic}} + A_{\mathrm{aq}}\tau_{\mathrm{aq}}} \tag{2}$$

where

$$\varphi_{\mathrm{mic}} = \int_0^\infty \exp\Big(-t/\tau_{\mathrm{mic}} - C[1 - \exp(-k_q t)]\Big)dt \tag{3}$$

The decay curves of pyrene emission in PLA-QPDMAEA aqueous solutions and their fits to the the decay model (eq.1) are shown in the Supporting Information (Fig. S1 in Section S1). The pyrene lifetime in the aqueous pseudophase was fixed at the value obtained for pyrene in aqueous buffer, $\tau_{\mathrm{aq}} = 131\,\mathrm{ns}$.

The values of f_{mic} and k_{q} obtained from the fits are plotted in Fig. 3 as functions of PLA-QPDMAEA concentration, $c_{\mathrm{PLA-QPDMAEA}}$. The f_{mic} decreases with decreasing $c_{\mathrm{PLA-QPDMAEA}}$ indicating the decreasing amount of pyrene solubilized in PLA-QPDMAEA micelles. The steep decrease of the quenching constant at $c_{\mathrm{PLA-QPDMAEA}} = 0.01\,\mathrm{g/l}$ can be ascribed to the dissociation of micelles below the CMC. For $c_{\mathrm{PLA-QPDMAEA}} \leq 0.01\,\mathrm{g/l}$, the solution contains only PLA-QPDMAEA unimers and the faster component of the decay cannot be any longer interpreted by means of the micellar quenching model. Above the CMC, both τ_{mic} and C change ($44 - 57\,\mathrm{ns}$ and 0.6–1.4, respectively, see Fig. S1 in ESI), indicating that the dynamics of pyrene quenching in the micellar pseudophase is dependent on PLA-QPDMAEA concentration.

For the ideally behaving system of two pseudophases and integral emission intensity fractions proportional to fluorophore amounts in the pseudophases, the $f_{\mathrm{mic}}/f_{\mathrm{mic}} = f_{\mathrm{mic}}/(1–f_{\mathrm{mic}})$ should be proportional to $c_{\mathrm{PLA-QPDMAEA}}$. However, the plot in the insert of Fig. 3 shows

substantial deviation from proportionality at higher PLA-QPDMAEA concentration, which can be ascribed to heterogeneity of the micellar pseudophase (the mixture of spherical and cylindrical micelles) and to changes of the micellar morphology by gradual transition of spherical micelles to cylindrical with increasing PLA-QPDMAEA concentration. This trend allows us to not only determine the critical micelle concentration but also show that such micelles with a PLA soft core can be dynamically formed and disassembled and thus used for efficient encapsulation of low-molar mass compounds.

Co-assembly of PLA-QPDMAEA and PEO-PMAA copolymers

Our observations confirmed that the PLA-QPDMAEA copolymer formed reversible micelles, and therefore they should also form reversible complexes with an oppositely charged diblock PEO-PMAA composed of a neutral hydrophilic PEO block and an anionic PMAA block. The PMAA block should form an interpolyelectrolyte complex (IPEC) with the QPDMAEA block, whereas the hydrophilic PEO block should form an outer shell stabilizing the complexes in solution, resulting in multilayered structures with a soft PLA layer and an IPEC layer.

To study the assembly of PLA-QPDMAEA micelles with PEO-PMAA, we prepared aqueous solutions in 50 mM sodium tetraborate (pH 9.2) to ensure the full ionization of the PMAA block and to keep ionic strength constant to eliminate its effect on IPEC formation. We varied the molar ratio [MAA]/[QDMAEA] to control the excess charge in the IPEC layer. We used two PEO-PMAA copolymers with different block lengths: 'short' $PEO_{375} - PMAA_{38}$ and 'long' $PEO_{697} - PMAA_{476}$, schematically shown in Fig. 1, to assess the effect of the block length of the copolymer on its ability to form IPEC and on the stability of the resulting complexes in aqueous solution. The long PEO blocks are aimed to stabilize formed complexes in aqueous solution, the short PMAA block has a length similar to the length of PLA block, while the long PMAA was chosen to be 10 times longer than PLA block to provide an excess of negative charge.

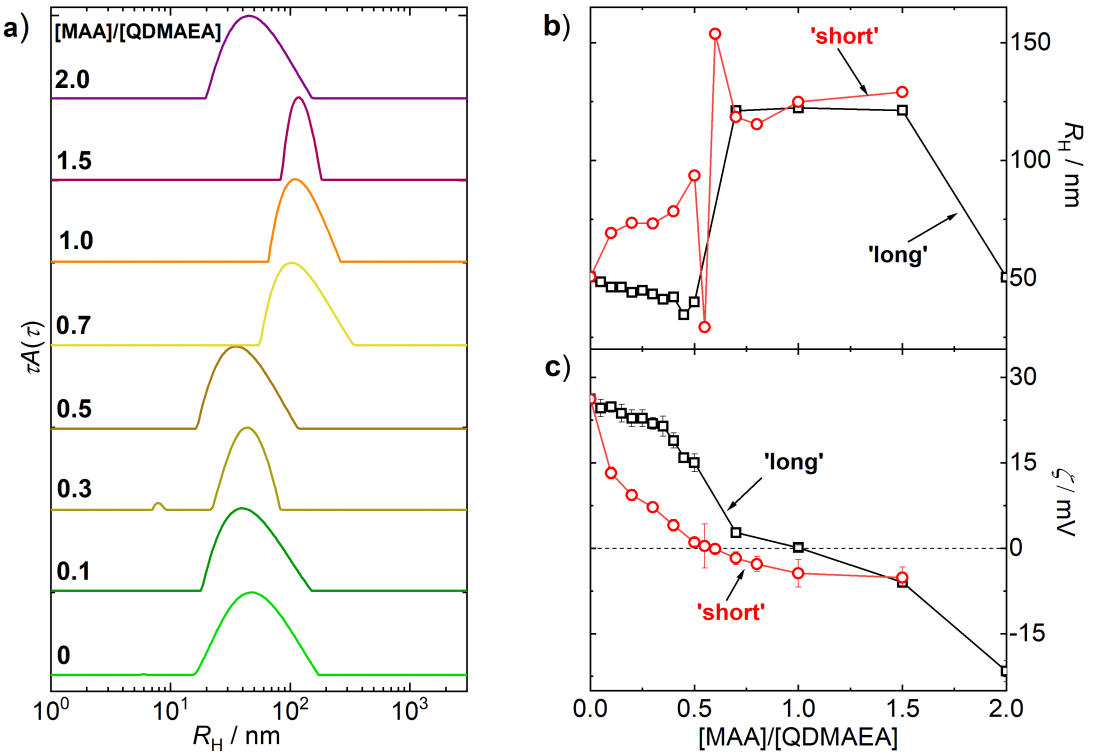

Figure 4: (a) DLS distributions of hydrodynamic radii, R_{H}, of complexes of PLA-QPDMAEA with 'long' PEO-PMAA. The charge ratios [MAA]/[QDMAEA] of complexes are indicated above each curve. (b) Mean apparent hydrodynamic radius, R_{H}, and (c) Zeta-potential, ζ, for PLA-QPDMAEA/PEO-PMAA complexes as functions of [MAA]/[QDMAEA].

Light scattering (LS) techniques were used to study the interaction of these two copolymers at various charge ratios, i.e., the ratios of negatively charged monomeric units to positively charged ones [MAA]/[QDMAEA]. Fig. 4a shows the distribution of hydrodynamic radii for the mixture of PLA-QPDMAEA and long PEO-PMAA at the scattering angle $\theta = 90°$, R_{H} (the distributions for complexes with short PEO-PMAA are shown in Fig.S3 in Section 2.1.1, ESI). DLS showed that the pure PLA-QPDMAEA copolymer formed particles with a unimodal size distribution in aqueous solution. After adding the oppositely charged PEO-PMAA, the distribution of R_{H} remained unimodal, albeit shifted to higher R_{H} values at a charge ratio [MAA]/[QDMAEA] > 0.5.

For complexes with a long PEO-PMAA, the mean apparent value of R_{H} (Fig. 4b) decreased slightly from 50 nm to 35 nm up to a charge ratio [MAA]/[QDMAEA] $= 0.5$, whereas

the ζ-potential (Fig. 4c) decreases from +25 mV to +15 mV. These observations confirm the complexation of two oppositely charged blocks as shown by the collapse of the particles due to the formation of a compact IPEC layer and by the decrease in the charge on the surface of the particles. Further addition of oppositely charged copolymer leads to a sharp increase in particle size up to 120 nm and to a decrease in ζ-potential to −22 mV, indicating a morphological transition of the complexes and formation of a new negatively charged outer layer. The negative sign of the ζ-potential likely derives from the excess of PMAA in the outer shell.

For the complexes formed by short PEO-PMAA, the R_{H} of the particles increased from 50 to 80 nm after each addition of PEO-PMAA up to a charge ratio [MAA]/[QDMAEA] = 0.5 followed by a sharp decrease in R_{H} above this point, likely caused by the collapse of polyelectrolyte chains. The ζ-potential decreased to 0 mV, thus indicating that the complexes with short and long PEO-PMAA copolymers are formed through different mechanisms related to a different mutual arrangement of the chains in the outer shell that leads either to the formation of a loose shell or to the collapse of the particle shell. Further increasing the charge ratio lead to the precipitation of the complexes. Therefore, DLS and ELS measurements of these samples were performed after removing the precipitate by centrifugation. These measurements showed that the particles in solution have the same R_{H} as the complexes with long PEO-PMAA copolymers (ca. 120 nm) with negative ζ-potential at the surface of the resulting particles. Thus, the increase in particle size and simultaneous decrease in their surface charge confirmed the formation of complexes between PLA-QPDMAEA and PEO-PMAA.

To reveal the role of the fluid PLA core, we compared the complexation of PLA-QPDMAEA micelles with that of micelles of the polystyrene-*block*-poly(2-methylvinylpyridinium iodide) ($PS_{228} - QPVP_{53}$) with 'long' and 'short' PEO-PMAA diblock copolymers. The amphiphilic PS-QPVP copolymer contains a PS block with a high $T_{\mathrm{g}} = 325$ K and forms core/shell micelles with a solid PS core and a positively charged QPVP shell. The core/shell micelles were

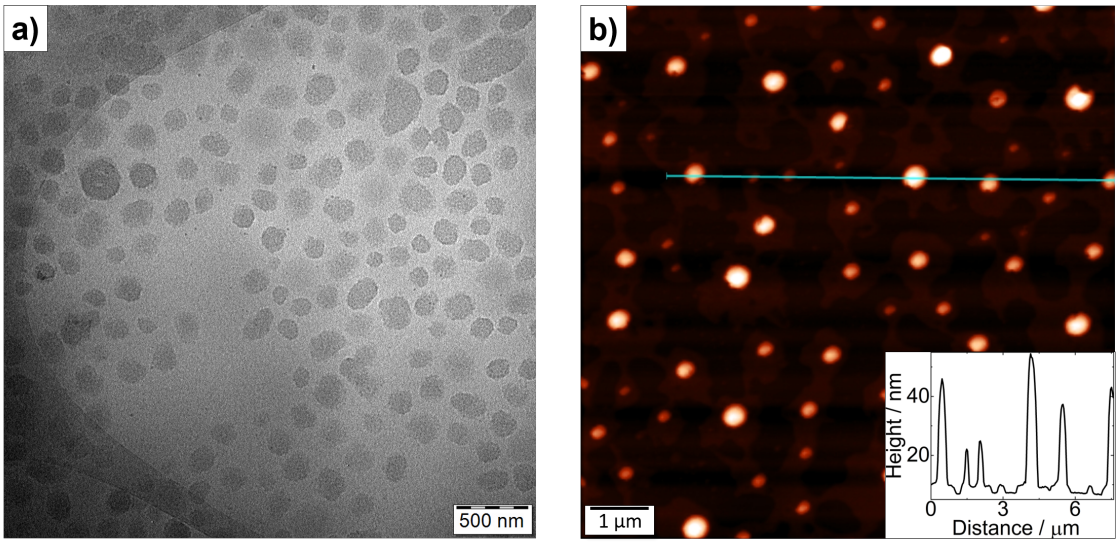

Figure 5: (a) Cryo-TEM micrograph of PLA-QPDMAEA/PEO-PMAA complexes at [MAA]/[QDMAEA] =1.0. (b) AFM scan of aggregates at a charge ratio of 1.5 deposited on a mica surface. Inset: section analysis.

prepared by nanoprecipitation of the PS-QPVP diblock copolymer because such a copolymer cannot self-assemble into core/shell micelles otherwise in aqueous solution. The scattering intensity of the mixture of PS-QPVP and PEO-PMAA (see Fig. S5 in Section 2.1.2, ESI) increased even at a low charge ratio [MAA]/[QVP], and the mixture started to precipitate at charge ratios [MAA]/[QVP]=0.02 for complexes with short PEO-PMAA copolymer and at [MAA]/[QVP]=0.03 for complexes with long PEO-PMAA copolymer. These results indicated that micelles with a kinetically frozen core are not able to form stable IPEC complexes similar to those of micelles with a soft PLA core. The formation of such IPECs in solution requires the reorganization of the chains inside core/shell micelle, which becomes possible only for the micelles with a soft core.

The size and shape of the PLA-QPDMAEA/PEO-PMAA particles were further confirmed by both cryo-TEM and AFM experiments. The TEM micrograph (Fig. 5a) shows that particles formed by PLA-QDMAEA with long PEO-PMAA copolymer have a spherical-like shape with an average radius of approximately $90 \pm 25\,\mathrm{nm}$ for the complex with a [MAA]/[QDMAEA] = 1.0, which is smaller than the value of R_H determined by DLS be-

cause of the low contrast for polymeric micelles in TEM in which the loose outer shell may not be visible. AFM was measured for the complexes at a [MAA]/[QDMAEA] = 1.5 to ensure the negative surface charge of the nanoparticles, since the positively charged species tend to form secondary aggregates on the negatively charged mica. The AFM scans showed (Fig. 5b) that particles absorbed on freshly cleaved-off mica surface also have spherical-like shape, but they are strongly flattened, with a diameter in the range of $300 - 500\,\text{nm}$ and height in the range of $20 - 40\,\text{nm}$. The AFM height scan and the cross-section analysis for an individual particle are shown in Fig. 6a and Fig. 6b. The height of the middle part of the particle (17 nm) is lower than the height of outer part (19 and 26 nm) indicating the presence of the soft core.

Simultaneously, the AFM phase scan of these complexes at a charge ratio of 1.5 (Fig. 6c) revealed the multilayered structure of the particles that became visible due to differences in mechanical properties of the layers. The section profile of the phase scan (Fig. 6d) shows that the particles consist of at least 3 layers: a soft core of 165 nm diameter, a stiff shell of 45 nm thickness and an outer soft shell of 25 nm thickness.

To gather more detailed information about the inner structure of the PLA-QPDMAEA/PEO-PMAA, we measured ^{1}H NMR spectra of the PLA-QPDMAEA/PEO-PMAA complexes at various charge ratios, as shown in Fig. 7. Adding the oppositely charged copolymer broadens the peak corresponding to the positively charged $N(CH_3)_3^+$ group of the QPDMAEA block (at chemical shift, $\delta = 3.2\,\text{ppm}$), which does not overlap with the proton spectrum of PEO-PMAA. Such an observation indicates that the formation of complex particles is accompanied by changes in the chemical environment of the positively charged groups[35] that loose mobility because of the interaction with carboxylic COO^- groups and formation of the interpolyelectrolyte complexes. After adding PEO-PMAA, the signal corresponding to PEO appears in the NMR spectrum, but the signals of PMAA protons do not, which confirms that the PMAA block is involved in the formation of a new layer and that the PEO block is localized in the outer shell. Due to the fluidity of PLA core, signals of PLA protons appear

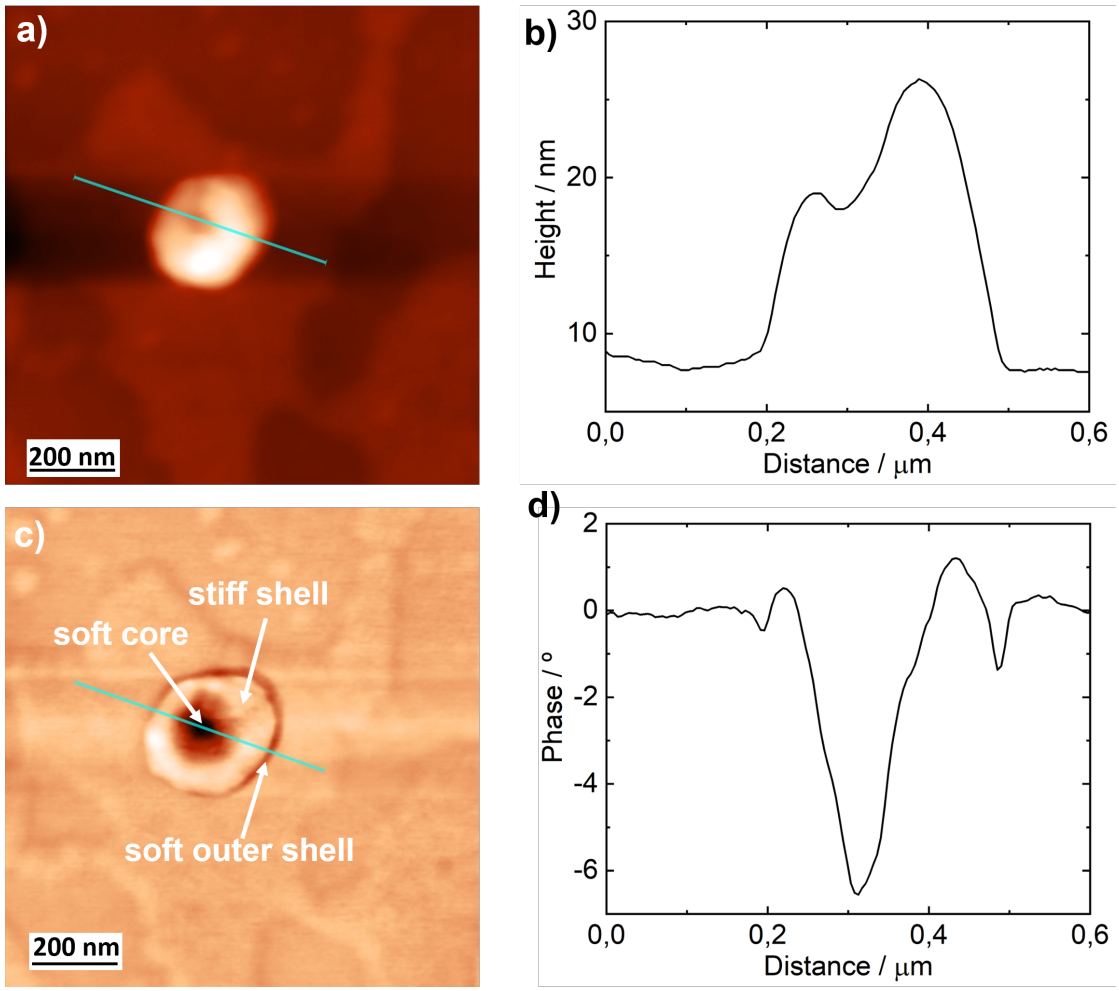

Figure 6: (a) AFM height scan, (b) phase scan and (c,d) section analysis of PLA-QPDMAEA/PEO-PMAA aggregates at [MAA]/[QDMAEA]=1.5.

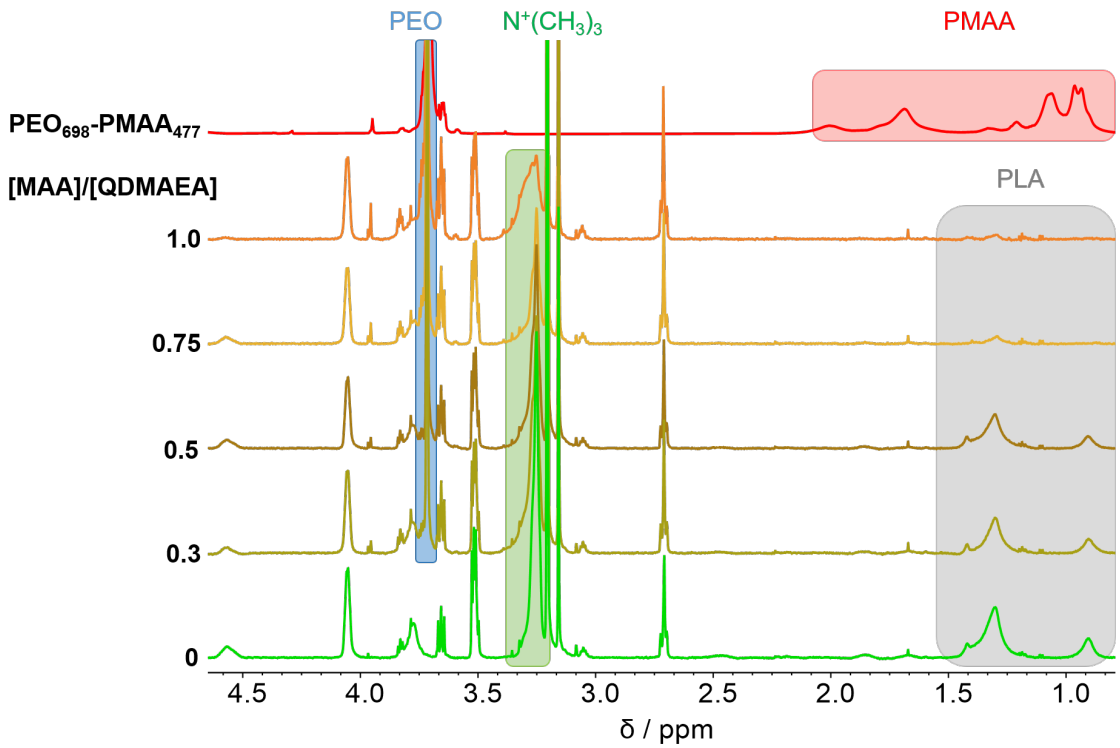

Figure 7: ^{1}H NMR spectra of PLA-QPDMAEA/PEO-PMAA complexes at various charge ratios.

in ^{1}H spectra, even in aqueous solution, in contrast to micelles with a solid core. The signal from protons of the PLA block at $1-2$ ppm disappears at high charge ratios because of the formation of a rigid QPDMAEA/PMAA layer next to a PLA layer that makes PLA chains less mobile. Thus, the ^{1}H NMR experiment demonstrated the formation of particles with PLA layer followed by a QPDMAEA/PMAA IPEC layer and an outer shell composed of the PEO.

Additional details about the inner structure of these multicompartment particles formed by PLA-QPDMAEA and PEO-PMAA were obtained by SANS for complexes at various [MAA]/[QDMAEA] charge ratios (Fig. 8). Adding the oppositely charged 'long' PEO-PMAA copolymer to the core/shell micelles (mixture of spherical and cylindrical particles) did not significantly affect the shape of scattering curves up to a charge ratio of 0.5 (Fig. 8a); simultaneously, both the forward scattering, I, and the radius of gyration, R_g, increased slightly (Fig. 9a). Therefore, the addition of a small amount of PEO-PMAA did not lead

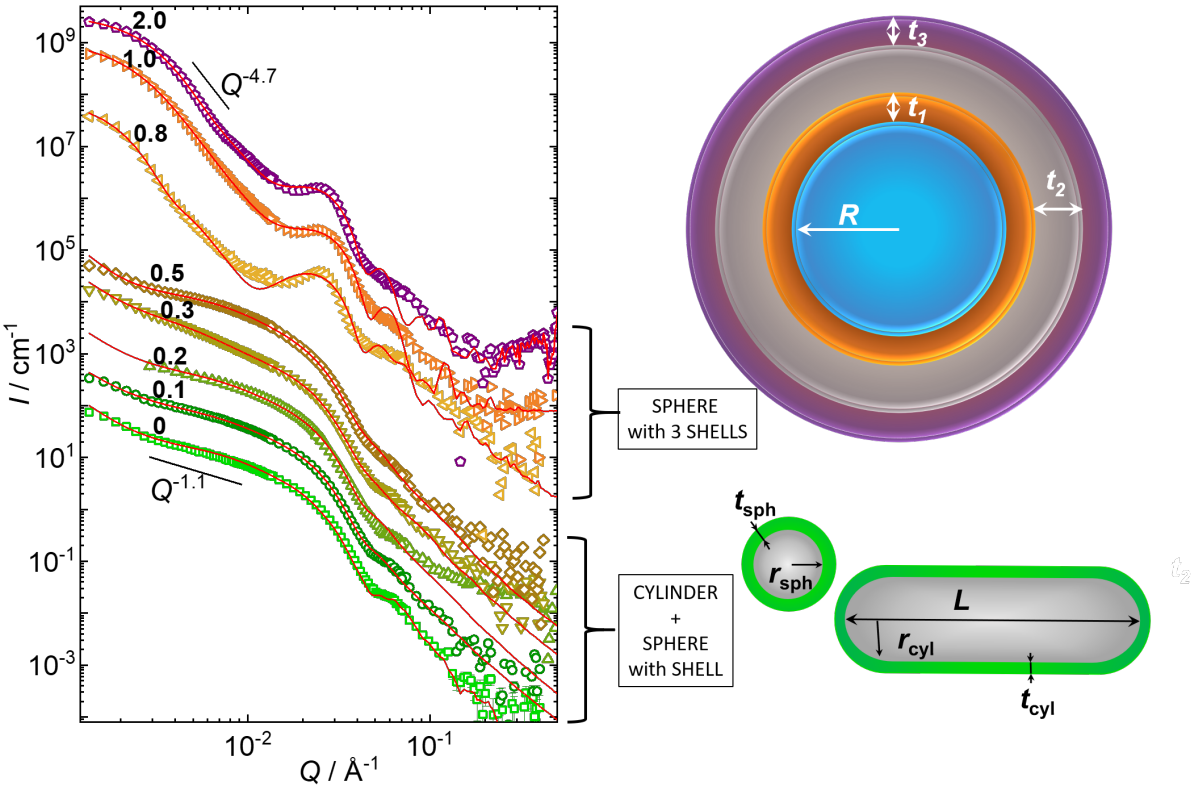

Figure 8: (left) SANS curves for PLA-QPDMAEA/PEO-PMAA solutions at various charge ratios indicated at each curve. The red lines represent fits of the curves using the block copolymer micelle model for an [MAA]/[QDMAEA] of up to 0.5 and the 4-layer micelle model for charge ratios higher than 0.5. (right) Schematic representation of the fitting models; the grey color represents the hydrophobic PLA core or layer, green - the positively charged QPDMAEA shell, orange - the inner QPDMAEA/PMAA IPEC layer, blue - the neutral hydrophilic PEO core and purple - the outer IPEC layer.

to the formation of a closely packed PMAA/QPDMAEA layer with a clear interface, but it led to a formation of a loose outer PMAA/QPDMAEA shell because of the presence of uncompensated positive QPDMAEA charge ($\zeta > 0$, Fig. 4c). Further increasing the PEO-PMAA concentration leads to a morphology transition and to the appearance of a correlation peak in the SANS curves. The change in the slope of the curves from -1 to -4 confirms the transition from cylindrical to compact spherical particles, in line with the TEM images. Simultaneously, R_g and the forward scattering intensity increase ca. 5 times, thus indicating the formation of large structures.

The SANS curves up to a charge ratio of 0.5 were fitted with the same linear combination of models as that used for pure PLA-QPDMAEA copolymer (a randomly oriented cylindrical shell with a circular cross-section and a spherical core surrounded by a shell, see description of the models in ESI, Section 2.5.1). The shells of both spherical and cylindrical micelles become thicker when adding the PEO-PMAA copolymer (Fig. 9b), thus confirming IPEC formation. The thickness of the shell of the spherical micelles, t_{sph} increases from 2 to 4 nm, whereas the thickness of the shell of cylindrical micelles t_{cyl} increases from 2 to 9 nm, indicating that the morphological transition is more favorable for cylindrical micelles.

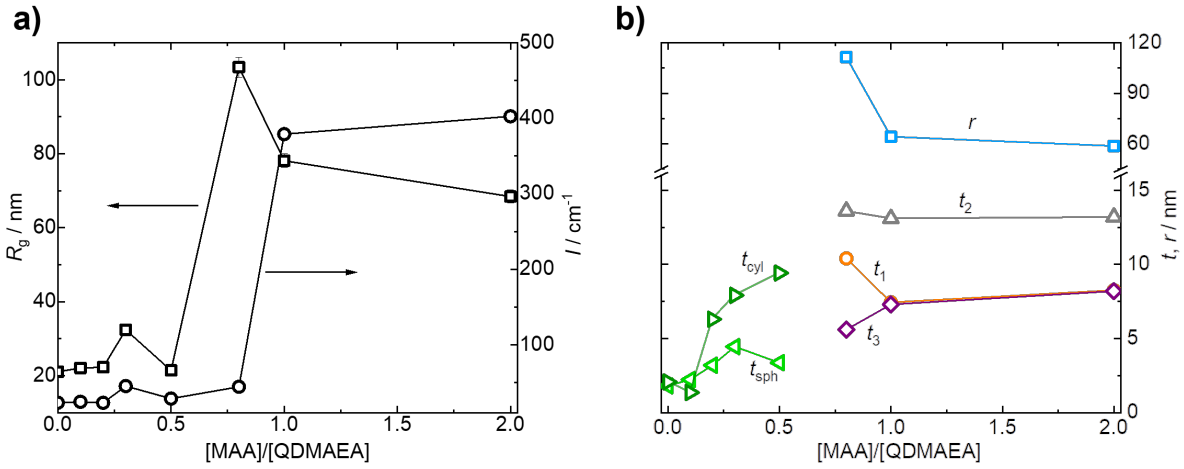

Figure 9: (a) Gyration radius, R_{g}, forward scattering intensity, I, and (b) thicknesses of shells of cylindrical and spherical micelles, t_{cyl} and t_{sph}, for [MAA]/[QDMAEA] from 0 to 0.5, the radius of the core, r, and the thicknesses of first, second and third shells, t_1, t_2, and t_3, for [MAA]/[QDMAEA] from 0.8 to 2.0 as assessed by fitting SANS curves.

Curves of the complexes with a charge ratio higher than 0.5 were fitted using the model of a micelle with the spherical core surrounded by four layers; the choice of the model, description of the model and the fitting procedure are described in the ESI (Section S2.5 and S2.6). The fits, shown in Fig. 8, revealed that at [MAA]/[QDMAEA] = 0.8 the particles consist of a core with a 110 nm radius followed by a first inner shell of 11 nm, a second shell of 13 nm and a third shell of 5 nm thickness. At higher ratios the radius of the core and the thickness of the inner layers (first and second) decreased, thus indicating that the layers became more compact. Simultaneously, the thickness of the outermost layer slightly

increased due to further complexation. Such a large core of more than 100 nm in diameter cannot be formed by the short PLA block alone, consisting of only 24 monomeric units. Only the PEO block is long enough to form the core, suggesting a transition from core/shell micelles with a fluid PLA core and a cationic QPDMAEA shell to vesicle-like multilayered micelles with a PEO core, a first IPEC layer followed by a PLA layer, then another IPEC layer and finally a loose PEO outer shell. Since the radius of the core is similar to the length of a fully stretched PEO block, the PEO core contains high amount of water that was confirmed by high scattering length density (SLD) values obtained by fitting SANS curves (Table S3, ESI). The SLD values calculated by fitting the experimental curves for all layers (see Table S3 in Section 2.6.2, ESI) differ from those calculated based on their assumed compositions (Section S2.6, ESI), indicating that all layers are swollen. The contrast variation in SANS measurements performed for PLA-QPDMAEA/PEO-PMAA complexes at different H_2O/D_2O ratios (Section S2.7, ESI) showed that the SLD values decrease linearly with increasing concentration of H_2O that confirms the presence of high amount of water molecules in each layer and, therefore, SLD values cannot be used to reveal their composition due to the unknown degree of swelling of each layer. Similar results were found when analyzing the short PEO-PMAA copolymer (see ESI), for which the form factor was similar to that of pure PLA-QPDMAEA for complexes up to a charge ratio of 0.3 and with morphology transition at charge ratio of 0.5. It is worth mentioning that one of the factors which may contribute to the formation of lamellar (or multilayered) morphology is dispersity of co-assembled copolymers. Luo and Eisenberg[36] pointed out that formation of vesicles is favorable for disperse block copolymers because the curved lamellar morphology is stabilized by segregation of long and short corona chains outside and inside the vesicle.

To help us understand the composition of layers within the multicompartment particles, we used the Scheutjens-Fleer Self-Consistent Field (SF-SCF)[37,38] modeling to predict the equilibrium structure of the nanoparticles. In this model, we represented the copolymers as schematically shown in Fig. 10. The model is semi-quantitative, accounting for the hy-

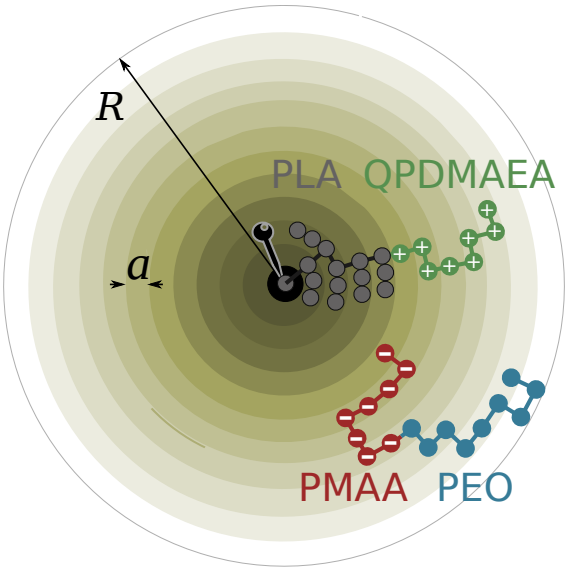

Figure 10: Schematic representation of the SCF model for the system containing PLA-QPDMAEA and PEO-PMAA block copolymers.

drophobic character of PLA, for charges of the PMAA and QDMAEA segments, and for the approximate size of the segments, determined by the lattice size a. The system is represented by a lattice composed of concentric spherical shells (layers) separated by a fixed distance a. By applying the spherical symmetry approximation, we explicitly consider the radial variation of the properties, while simultaneously assuming that properties within each layer are homogeneous. The spherical symmetry approximation enables fast and efficient calculation, but it also sets the fundamental limitation of the model.

Fig. 11a shows the density profiles of the structures formed by self-assembly of pure PLA-QPDMAEA, derived from the SF-SCF calculations. These profiles correspond to a micelle with a core composed of PLA, surrounded by a shell composed of QPDMAEA. Volume fraction of PLA in the core is close to 1.0 and decays quickly beyond a distance of $R \approx 8\,\mathrm{nm}$, indicating the core-shell interface. The volume fraction of QPDMAEA in the shell is much lower and decays gradually up to a distance of $R \approx 15\,\mathrm{nm}$, indicating a shell thickness of $t_1 \approx 8\,\mathrm{nm}$. Because the SCF model is only qualitative, these sizes should not be directly compared with the experimentally determined values. Instead, they should be compared with the results of SCF calculations at other compositions.

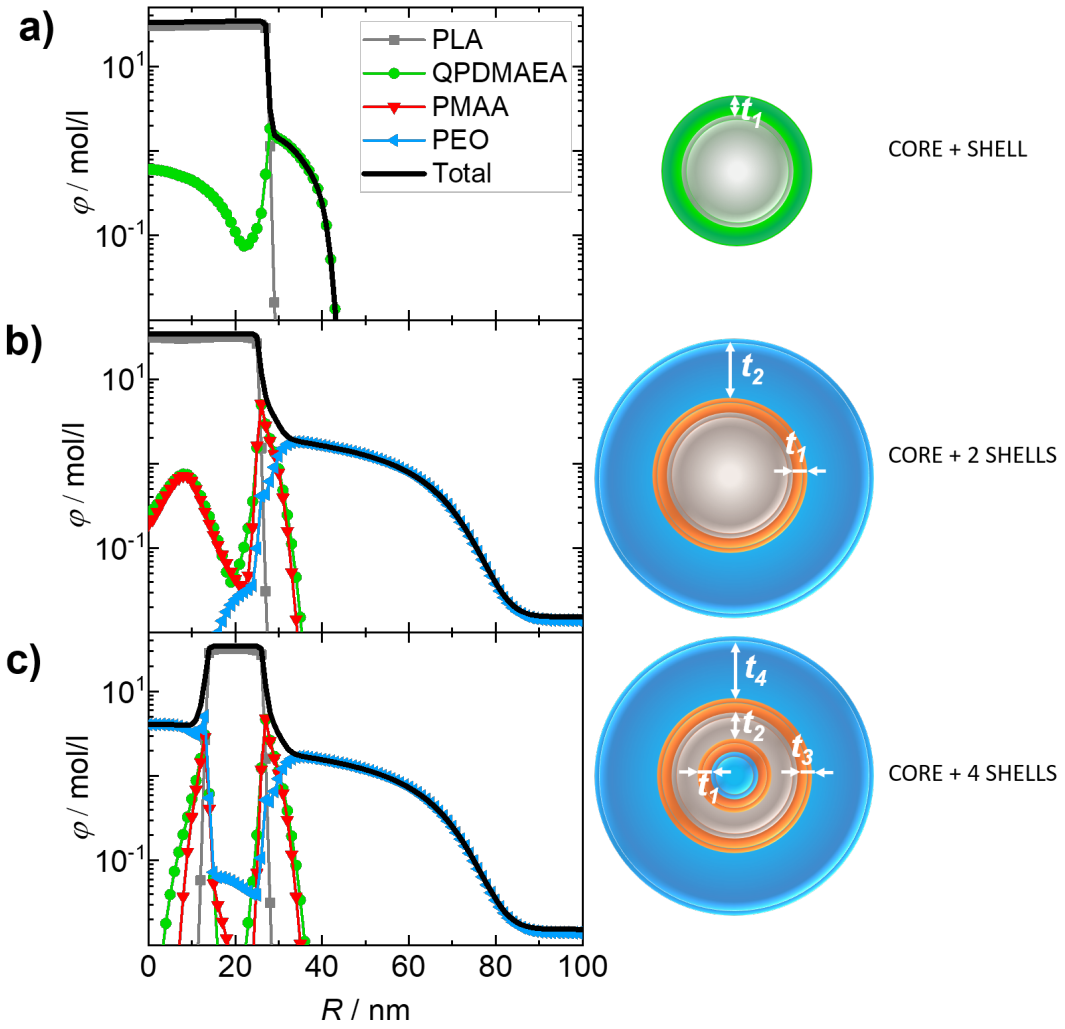

Figure 11: (left) Density profiles obtained from SCF calculations (a) for pure PLA-QPDMAEA, (b) and (c) for PLA-QPDMAEA/PEO-PMAA at charge ratios [MAA]/[QDMAEA] = 1.0. (right) Schematic representations of the formed particles reconstructed from SCF density profiles, where grey color corresponds to the hydrophobic PLA layer, green - the positively charged QPDMAEA shell, orange - the QPDMAEA/PMAA complex and blue - the neutral hydrophilic PEO layer.

Fig. 11b and Fig. 11c show the density profiles of the structures formed by a mixture of PLA-QPDMAEA and PEO-PMAA, at a charge ratio [MAA]/[QDMAEA] = 1.0 (analogous figures at other values of charge ratio are provided in Section 3, ESI). The profile in Fig. 11b corresponds to a three-layer micelle with a core consisting of PLA with a radius of $R \approx 8\,\text{nm}$, which is similar to that of pure PLA-QPDMAEA micelles. The middle layer consists of an interpolyelectrolyte complex of QPDMAEA and PMAA with much higher polymer volume fraction and thickness values, $t_1 \approx 5\,\text{nm}$ which are lower than the corresponding values of the shell of pure PLA-QPDMAEA micelles. Finally, the outer shell consists of PEO with a gradually decaying density up to $R \approx 25\,\text{nm}$, indicating a shell thickness of $t_2 \approx 15\,\text{nm}$. The profile in Fig. 11c corresponds to a four-layer micelle with a core composed of hydrated PEO at a volume fraction of $\phi \approx 35\,\text{mol/l}$ and with a radius of $R \approx 3\,\text{nm}$. The first layer with a thickness of $t_1 \approx 5\,\text{nm}$ consists of PEO and an interpolyelectrolyte complex of QPDMAEA and PMAA. The second layer with a thickness $t_2 \approx 12\,\text{nm}$ consists of almost pure PLA, followed by a third layer, whose composition and thickness are similar to those of the second layer, albeit with less PEO. The remaining PEO extends beyond the third layer and forms an outer shell of the micelle with a thickness of $t_4 \approx 30\,\text{nm}$. Notably, the profiles in Fig. 11b and Fig. 11c were obtained under the same conditions, through calculations differing only in overall system size. The SCF calculations converge in the profiles of three- or four-layered micelles, depending on the system size. Both types of profiles yield similar values of free energy per chain, creating an oscillating pattern as a function of system size (see Section 3 in ESI for additional details). The preference of one or the other profile is likely an artifact of the discretization to layers, in combination with the assumption of spherical symmetry. The former is an inherent feature of the SF-SCF model and cannot be avoided. The latter is most likely not fulfilled in four-layered micelles with PEO in the core. Therefore, our SCF calculations suggest that either three- or four-layered micelles should be formed, but we cannot reliably discern which structure is preferred over the other.

The comparison of our SCF calculations with the experimental data confirmed the for-

mation of micelles from pure PLA-QPDMAEA copolymer, the formation of three-layered micelles at a low charge ratio [MAA]/[QDMAEA] = 0.5, and the structural transition to multilayered micelles at a higher charge ratio [MAA]/[QDMAEA] = 1.0. The SCF model is not detailed enough to predict the correct size of the structures, but it reveals their key qualitative features. For multilayered micelles, the calculations revealed a structure in qualitative agreement with the results from the fit of the SANS data. The modeling supported the hypothesis that was previously formulated based on these fits. More specifically, the modeling revealed four-layer micelles with PEO in the core, with first and third layers of very similar thickness but slightly different composition, consisting of IPECs. The first and third layers are separated by the second layer composed of pure PLA. Lastly, the outermost layer predicted by the numerical model has a much lower polymer density than the other layers and thus may not be clearly revealed by scattering experiment due to insufficient contrast.

Conclusions

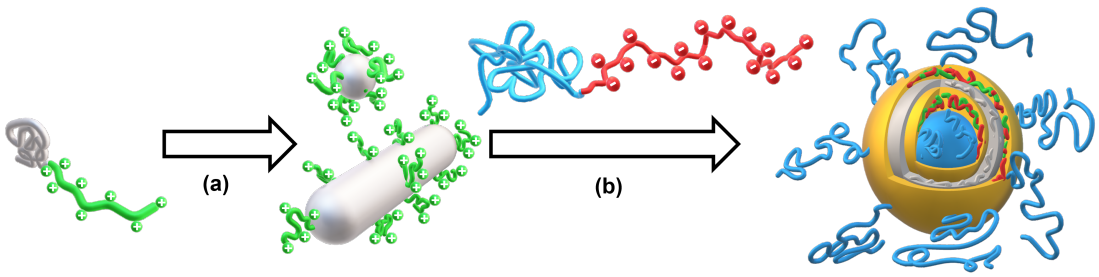

Figure 12: (a) Self-assembly of PLA-QPDMAEA into core/shell micelles with a fluid spherical and cylindrical PLA core and a positively charged QPDMAEA shell and (b) Interpolyelectrolyte complex formation of PLA-QPDMAEA core/shell micelles with PEO-MAA and formation of multilayered micelles with a PEO core, an IPEC inner layer, a soft middle layer, an IPEC outer layer and a hydrophilic neutral corona.

We studied the self-assembly of an amphiphilic diblock copolymer (PLA-QPDMAEA) containing a PLA block with a low glass transition temperature and characterized the corresponding particles by DLS, ELS, TEM and SANS. We showed that PLA-QPDMAEA copolymer self-assemble in aqueous solution, forming spherical and cylindrical core/shell micelles with a soft PLA core and a positively charged QPDMAEA shell. Due to the fluidity of the core, these micelles are able to encapsulate and release hydrophobic solutes efficiently and to assemble and disassemble dynamically,as shown by time-resolved fluorescence spectroscopy analysis of pyrene release. Moreover, we showed that PLA-QPDMAEA core/shell micelles form complexes with an oppositely charged, double hydrophilic block copolymer (PEO-PMAA) with two different chain lengths, 'short' $PEO_{375} - PMAA_{38}$ and 'long' $PEO_{697} - PMAA_{476}$. By DLS, ELS TEM and AFM, we showed that they form large spherical particles with a surface charge, which depends on the charge ratio. Their multilayered structure and the presence of a core with at least 3 layers was demonstrated by AFM and SANS. The vesicle-like structure of the PLA-QPDMAEA/PEO-PMAA complexes was also predicted by self-consistent field computer modeling, which showed that these structures consist of a water-swollen PEO core, a soft PLA layer surrounded by two IPEC layers, and an outermost layer formed by a loose PEO corona, as schematically shown in Fig. 12. While

the triblock terpolymers or copolymers with a more complex morphology (such as miktoarm stars or comb copolymers) have been used for obtaining multicompartment nanoparticles in the literature,[39–41] our study shows that coassembly of simple linear diblock copolymers is also a viable strategy for the preparation of such nanostructures. Thanks to the ability to tune the size, charge, and stability of such multicompartment micelles, containing dynamic IPEC and fluid PLA layers, these micelles may be applied to deliver both hydrophobic and multivalent ionic solutes. The solubilization of both hydrophobic and multivalent ionic solutes in the multicompartment micelles and their release and influence of pH, ionic strength and block copolymer composition of the micelles on the release kinetics will be a subject of our future study.

Experimental Section

Materials

The poly(lauryl acrylate)-*block*-poly(trimethylammonioethyl acrylate iodide) diblock copolymer ($PLA_{24} - QPDMAEA_{18}$, $M_W = 11.3\,\mathrm{kgmol^{-1}}$, Fig. 1) is the quarternized analogue of poly(lauryl acrylate)-*block*-poly(dimethylaminoethyl acrylate) (PLA-PDMAEA) diblock copolymers (dispersity index determined by size-exclusion chromatography (SEC) is 1.41). The PLA-QPDMAEA diblock copolymers were prepared by a simple quarternization reaction in THF, using methyl iodide (CH_3I) as the quarternizing agent. This synthetic procedure has already been described in detail in our previous study.[29]

Details of the synthesis of the polystyrene-*block*-poly(2-methylvinylpyridinium iodide) diblock copolymer ($PS_{228} - QPVP_{53}$, dispersity 1.01) are reported in Meristoudi et al.[42] The poly(ethylene oxide)-*block*-poly(methacrylic acid) diblock copolymers ('short' $PEO_{375} - PMAA_{38}$ dispersity 1.08 and 'long' $PEO_{697} - PMAA_{476}$ dispersity 1.5) were purchased from Polymer Source, Inc.

Preparation of the particles

PLA-QPDMAEA copolymer was dissolved in 0.05 M aqueous sodium tetraborate ($Na_2B_4O_7$) and its concentration was adjusted to 1 g/l by weighing the solution. The polymer concentration 1 g/l was chosen to assure high signal-to-noise ratio in DLS, SANS and NMR measurements and avoid high turbidity and aggregation of the samples at the same time. The formed particles were stable for at least several weeks. DLS measurements were performed for PLA-QPDMAEA copolymer in different buffers (Fig. S2 in ESI); 0.05M sodium tetraborate was chosen as a solvent since no large aggregates were observed. All measurements were performed after stirring the solution for 24 hours to ensure equilibration of the solution and micelle formation. Stock solutions of double hydrophilic PEO-PMAA copolymers (ca. 10 g/l) in 0.05 M $Na_2B_4O_7$ were prepared similarly by solution weighting; small amounts of PEO-PMAA solutions (several microlitres) were added to the PLA-QPDMAEA solution upon stirring, then the sample was weighted to calculate the exact charge ratio values and then it was left standing for 1 h for equilibration prior to the measurements. The samples were filtered with 0.45 μm PVDF syringe filters only for light scattering measurements.

PS-QPVP micelles were prepared by nanoprecipitation method described below. Stock solution of PS-QPVP copolymer (ca. 10 g/l) was dissolved in dimethylformamide (DMF), slowly added drop-wise under vigorous stirring to a surplus of 0.05 M $Na_2B_4O_7$ to adjust the PS-QPVP concentration to 2 g/l. The resulting solution was dialyzed against 1 liter of 0.05 M aqueous sodium tetraborate and diluted to adjust the polymer concentration to 1 g/l.

Methods

Dynamic Light Scattering (DLS). The dynamic light scattering setup (ALV, Langen, Germany) consisted of a 22 mW He–Ne laser ($\lambda = 632.8$ nm), an ALV CGS/8F goniometer, an ALV High QE APD detector, and an ALV 5004 multi-bit, multi-tau autocorrelator. The DLS measurements were performed at 25°C at a scattering angle of $\theta = 90°$. DLS measurements for all systems were analyzed by fitting the normalized time autocorrelation function of the

scattered light intensity using the constrained regularization algorithm (CONTIN)[43] because of the complexity of the polymeric particles and the co-existence of 2 fractions of particles. The copolymer mass concentration in the solution was $c_{\mathrm{pol}} = 1.0\,\mathrm{g\,L^{-1}}$. The samples were filtered using $0.45\,\mu$m Acrodisc PVDF membrane filters before the measurements.

Electrophoretic Light Scattering (ELS). Zeta-potential measurements were performed with a Nano-ZS Zetasizer (Malvern Instruments, U.K.) at 25°C. The value of the electrophoretic mobility, μ, was averaged over three subsequent measurements, each of which consisting of 15 runs, and used to calculate the zeta-potential values, ζ, from the Henry equation in the Smoluchowski approximation, $\mu = \epsilon\zeta/\eta$, where μ is the electrophoretic mobility and ϵ is the dielectric constant of the solvent.

Small-Angle Neutron Scattering (SANS). SANS experiments were performed at FRM II, Garching, Germany, on a KWS-2 small-angle scattering diffractometer.[44] The measurements were performed on a position-sensitive 2D detector consisting of an array of 128 ^{3}He tubes (pixel size 8 mm) using a nonpolarized, mono-chromatic (wavelength, λ with a distribution $\Delta\lambda = 10\%$, set by a velocity selector) incident neutron beam collimated with rectangular apertures for two sample-to-detector distances, namely 2, 8, and 20 m (λ= 0.6 nm). Using this setup, the 0.015-4.6 $\mathrm{nm^{-1}}$ q-range was investigated, finding isotropic 2-dimensional scattering patterns, which were azimuthally averaged, thereby expressing the variation of the scattered intensity $I(q)$ as a function of the momentum transfer $q = 4\pi \sin\theta/\lambda$, where 2θ is the scattering angle. The curves were corrected for the dark current, for the background scattering from the empty cell and for detector efficiency. Helma quartz cells 1- and $2-$ mm-thick were used for these experiments, which were performed in 50 mM sodium tetraborate in D_2O. The buffer was measured separately, subtracting the scattering from the buffer.

Atomic force microscopy (AFM). Atomic force microscopy measurements were performed in tapping mode under ambient conditions using a NT-MDT Ntegra Prima scanning probe microscope, equipped with a Nanosensors silicon cantilever. The samples were prepared by fast dip coating of a freshly peeled out mica surface. After evaporating their water, we dried

the samples in a vacuum oven at ambient temperature for ca. 5 hours.

Cryogenic Transmission Electron Microscopy (cryo-TEM). TEM micrographs for PLA-QPDMAEA copolymers and PLA-QPDMAEA/PEO-PMAA complexes were acquired on a Techain G2 Spirit Twin 12 microscope (FEI, Czech Republic) equipped with a cryo-attachment (Gatan, CA, USA). In total, 3 μL of the sample solution was dropped on an electron microscopy grid covered with a holey carbon supporting film (Electron Microscopy Science), which was hydrophilized just before the experiment by glow discharge (Expanded Plasma Cleaner, Harrick Plasma, USA). The excess of the solution was removed by blotting (Whatman no. 1 filter paper) for 1 s, and the grid was plunged into liquid ethane held at 181°C. The frozen sample was immediately inserted in the cryo-holder, transferred into the microscope and observed at −173°C using bright field imaging at an accelerating voltage of 120 kV.

Fluorometry . Fluorescence emission measurements were performed in 1 cm quartz cuvettes using a Fluorolog FL 3-22 fluorometer (Horiba Jobin Yvon, France) equipped with double-grating excitation and emission monochromators, a FluoroHub time-correlated single photon counting module and a TBX single photon counting detector. Fluorescence emission decays were measured using a 378 nm NanoLed diode laser source with a pulse FWHM of ca. 200 ps, operated at a repetition frequency of 1 MHz. Pyrene was dissolved in a small amount of methanol and further diluted in deionized water and then added to PLA-QPDMAEA in water ($c = 1$ g/l) to a pyrene concentration in the mixture of $\approx 10^{-6}$ M. The resulting mixture was diluted in water to the desired concentrations. Emission decays were measured at an emission wavelength of 450 nm in a time window of 57 ns with a resolution of 6.98 ps per channel.

Nuclear Magnetic Resonance (NMR). The ^{1}H NMR data of PLA-QPDMAEA and PLA-QPDMAEA/PEO-PMAA were recorded on a Bruker Avance III 600 MHz spectrometer at 25°C. The samples were prepared at a concentration of 15 gL^{-1} PLA-QPDMAEA in 50 mM borax solution in D_2O. All data were processed and fitted using the MestReNova software.

SCF model and method. We used the Scheutjens-Fleer Self-Consistent Field modeling[37,38] to investigate the self-assembly of our block copolymers, which were schematically represented as shown in Fig. 10. For simplicity, all polymer segments, except PLA, were treated as hydrophilic by setting $\chi = 0$, where χ is the Flory-Huggins parameter. PLA segments were defined as hydrophobic by setting $\chi = 2.7$. This value was estimated based on the Hansen solubility parameters,[45] as described in Section 3, in ESI. In addition, MAA segments were defined as negatively charged, and QDMAEA segments as positively charged. The length of each block was chosen to match the short PEO-PMAA block copolymers used in the experiments (Fig. 1). All calculations were performed assuming the spherical symmetry of the system. This assumption reduces the three-dimensional problem to a one-dimensional problem, thereby decreasing the computational requirements by several orders of magnitude. To determine the equilibrium structures, we performed a set of SCF calculations at fixed polymer concentrations but at different sizes of the simulation box. Then, we selected the structures that correspond to the minimum of free energy as a function of system size at a fixed overall composition. Additional technical details of the SCF calculations are provided in Section 3, ESI.

Acknowledgments

This research was supported by the Grant agency of the Charles University (GAUK), project No.1375219, by the Czech Science foundation, project No.19-10429S, by the Charles University Research Centre (Program No. UNCE/SCI/014) and by the Ministry of Education, Youth and Sports of the Czech Republic, Operational Program Research, Development and Education: "Excellent Research Teams", Project No. CZ.02.1.01/0.0/0.0/15_003/0000417-CUCAM. This project was also funded from the European Union's Horizon 2020 research and innovation programme under grant agreement No 731019 (EUSMI) to access to the KWS-2 instrument operated by JCNS at the Heinz Maier-Leibnitz Zentrum (MLZ), Garching,

Germany. The authors also thank the European Synchrotron Radiation Facility (ESRF), Grenoble, France for granting SAXS beam time (Project No. SC-4621 at the ID02 beamline). The help of Dr. Ewa Pavlova with cryo-TEM experiments and Dr. Carlos V. Melo with proofreading the manuscript is also gratefully acknowledged.

References

(1) Mura, S.; Nicolas, J.; Couvreur, P. Stimuli-responsive nanocarriers for drug delivery. *Nature Materials* **2013**, *12*, 991–1003.

(2) Bogomolova, A.; Hruby, M.; Panek, J.; Rabyk, M.; Turner, S.; Bals, S.; Steinhart, M.; Zhigunov, A.; Sedlacek, O.; Stepanek, P.; Filippov, S. K. Small-angle X-ray scattering and light scattering study of hybrid nanoparticles composed of thermoresponsive triblock copolymer F127 and thermoresponsive statistical polyoxazolines with hydrophobic moieties. *Journal of Applied Crystallography* **2013**, *46*, 1690–1698.

(3) Kaldybekov, D. B.; Filippov, S. K.; Radulescu, A.; Khutoryanskiy, V. V. Maleimide-functionalised PLGA-PEG nanoparticles as mucoadhesive carriers for intravesical drug delivery. *European Journal of Pharmaceutics and Biopharmaceutics* **2019**, *143*, 24–34.

(4) Kaberov, L. I.; Verbraeken, B.; Riabtseva, A.; Brus, J.; Radulescu, A.; Talmon, Y.; Stepanek, P.; Hoogenboom, R.; Filippov, S. K. Fluorophilic–Lipophilic–Hydrophilic Poly(2-oxazoline) Block Copolymers as MRI Contrast Agents: From Synthesis to Self-Assembly. *Macromolecules* **2018**, *51*, 6047–6056.

(5) Kedracki, D.; Filippov, S. K.; Gour, N.; Schlaad, H.; Nardin, C. Formation of DNA-Copolymer Fibrils Through an Amyloid-Like Nucleation Polymerization Mechanism. *Macromolecular Rapid Communications* **2015**, *36*, 768–773.

(6) Xu, Y.; Hu, W. Formation of Multicontinuous 3D Network Nanostructures with Increased Complexity in ABC-Type Block Copolymers. *Langmuir* **2020**, *36*, 11324–11331.

(7) Egli, S.; Schlaad, H.; Bruns, N.; Meier, W. Functionalization of Block Copolymer Vesicle Surfaces. *Polymers* **2011**, *3*, 252–280.

(8) Blanazs, A.; Armes, S. P.; Ryan, A. J. Self-assembled block copolymer aggregates: From micelles to vesicles and their biological applications. *Macromolecular Rapid Communications* **2009**, *30*, 267–277.

(9) Cabral, H.; Miyata, K.; Osada, K.; Kataoka, K. Block Copolymer Micelles in Nanomedicine Applications. *Chemical Reviews* **2018**, *118*, 6844–6892.

(10) Förster, S.; Antonietti, M. Amphiphilic Block Copolymers in Structure-Controlled Nanomaterial Hybrids. *Advanced Materials* **1998**, *10*, 195–217.

(11) Vriezema, D. M.; Comellas Aragonès, M.; Elemans, J. A. A. W.; Cornelissen, J. J. L. M.; Rowan, A. E.; Nolte, R. J. M. Self-Assembled Nanoreactors. *Chemical Reviews* **2005**, *105*, 1445–1490.

(12) Cui, H.; Chen, Z.; Zhong, S.; Wooley, K. L.; Pochan, D. J. Block Copolymer Assembly via Kinetic Control. *Science* **2007**, *317*, 647–650.

(13) Kataoka, K.; Harada, A.; Nagasaki, Y. Block copolymer micelles for drug delivery: design, characterization and biological significance. *Advanced Drug Delivery Reviews* **2001**, *47*, 113–131.

(14) Zhulina, E. B.; Borisov, O. V. Self-Assembly in Solution of Block Copolymers with Annealing Polyelectrolyte Blocks. *Macromolecules* **2002**, *35*, 9191–9203.

(15) Uchman, M.; Procházka, K.; Štěpánek, M.; Mountrichas, G.; Pispas, S.; Špírková, M.; Walther, A. pH-Dependent Self-Assembly of Polystyrene- block -Poly((sulfamate-carboxylate)isoprene) Copolymer in Aqueous Media. *Langmuir* **2008**, *24*, 12017–12025.

(16) Förster, S.; Abetz, V.; Müller, A. H. E. Polyelectrolyte Block Copolymer Micelles. *Advances in Polymer Science* **2004**, *166*, 173–210.

(17) Lísal, M.; Limpouchová, Z.; Procházka, K. The self-assembly of copolymers with one hydrophobic and one polyelectrolyte block in aqueous media: a dissipative particle dynamics study. *Physical Chemistry Chemical Physics* **2016**, *18*, 16127–16136.

(18) Skandalis, A.; Pispas, S. PDMAEMA-: B -PLMA- b -POEGMA triblock terpolymers via RAFT polymerization and their self-assembly in aqueous solutions. *Polymer Chemistry* **2017**, *8*, 4538–4547.

(19) Colombani, O.; Ruppel, M.; Burkhardt, M.; Drechsler, M.; Schumacher, M.; Gradzielski, M.; Schweins, R.; Müller, A. H. E. Structure of Micelles of Poly(n -butyl acrylate)-block -poly(acrylic acid) Diblock Copolymers in Aqueous Solution. *Macromolecules* **2007**, *40*, 4351–4362.

(20) Skandalis, A.; Pispas, S. PLMA-b-POEGMA amphiphilic block copolymers: Synthesis and self-assembly in aqueous media. *Journal of Polymer Science Part A: Polymer Chemistry* **2017**, *55*, 155–163.

(21) Pergushov, D. V.; Müller, A. H. E.; Schacher, F. H. Micellar interpolyelectrolyte complexes. *Chemical Society Reviews* **2012**, *41*, 6888.

(22) Katayose, S.; Kataoka, K. Water-Soluble Polyion Complex Associates of DNA and Poly(ethylene glycol)-Poly(l-lysine) Block Copolymer. *Bioconjugate Chemistry* **1997**, *8*, 702–707.

(23) Kabanov, A. V.; Bronich, T. K.; Kabanov, V. A.; Yu, K.; Eisenberg, A. Soluble Stoichiometric Complexes from Poly(N -ethyl-4-vinylpyridinium) Cations and Poly(ethylene oxide)- block -polymethacrylate Anions. *Macromolecules* **1996**, *29*, 6797–6802.

(24) Li, Y.; Bronich, T. K.; Chelushkin, P. S.; Kabanov, A. V. Dynamic Properties of Block Ionomer Complexes with Polyion Complex Cores. *Macromolecules* **2008**, *41*, 5863–5868.

(25) Murmiliuk, A.; Košovan, P.; Janata, M.; Procházka, K.; Uhlík, F.; Štěpánek, M. Local pH and Effective p K of a Polyelectrolyte Chain: Two Names for One Quantity? *ACS Macro Letters* **2018**, *7*, 1243–1247.

(26) Coelho, J. F. J.; Carvalho, E. Y.; Marques, D. S.; Popov, A. V.; Goncalves, P. M.; Gil, M. H. Synthesis of Poly(lauryl acrylate) by Single-Electron Transfer/Degenerative Chain Transfer Living Radical Polymerization Catalyzed by $Na_2S_2O_4$ in Water. *Macromolecular Chemistry and Physics* **2007**, *208*, 1218–1227.

(27) Agarwal, S.; Zhang, Y.; Maji, S.; Greiner, A. PDMAEMA based gene delivery materials. *Materials Today* **2012**, *15*, 388–393.

(28) Xiong, X.-B.; Falamarzian, A.; Garg, S. M.; Lavasanifar, A. Engineering of amphiphilic block copolymers for polymeric micellar drug and gene delivery. *Journal of Controlled Release* **2011**, *155*, 248–261, Proceedings of the Fifthteenth International Symposium on Recent Advances in Drug Delivery Systems.

(29) Raya, R. K.; Štěpánek, M.; Limpouchová, Z.; Procházka, K.; Svoboda, M.; Lísal, M.; Pavlova, E.; Skandalis, A.; Pispas, S. Onion Micelles with an Interpolyelectrolyte Complex Middle Layer: Experimental Motivation and Computer Study. *Macromolecules* **2020**, *53*, 6780–6795.

(30) Hamley, I. *Block Copolymers in Solution: Fundamentals and Applications*; John Wiley & Sons, Ltd: Chichester, UK, 2005; pp 173–213.

(31) Stuart, M. A. C.; Hofs, B.; Voets, I. K.; de Keizer, A. Assembly of polyelectrolyte-containing block copolymers in aqueous media. *Current Opinion in Colloid & Interface Science* **2005**, *10*, 30–36.

(32) Riess, G. Micellization of block copolymers. *Progress in Polymer Science* **2003**, *28*, 1107–1170.

(33) Li, N. K.; Fuss, W. H.; Tang, L.; Gu, R.; Chilkoti, A.; Zauscher, S.; Yingling, Y. G. Prediction of solvent-induced morphological changes of polyelectrolyte diblock copolymer micelles. *Soft Matter* **2015**, *11*, 8236–8245.

(34) Alargova, R. G.; Kochijashky, I. I.; Sierra, M. L.; Zana, R. Micelle Aggregation Numbers of Surfactants in Aqueous Solutions : A Comparison between the Results from Steady-State and Time-Resolved Fluorescence Quenching. *Langmuir* **1998**, *7463*, 5412–5418.

(35) Macdonald, P. M.; Tang, A. 1H and 2H NMR Studies of Poly(acrylate) and Poly(sodium styrenesulfonate) Interactions with Cationic Surfactant Micelles. *Langmuir* **1997**, *13*, 2259–2265.

(36) Luo, L.; Eisenberg, A. Thermodynamic Stabilization Mechanism of Block Copolymer Vesicles. *Journal of the American Chemical Society* **2001**, *123*, 1012–1013, PMID: 11456651.

(37) Fleer, G. J.; Stuart, M. A. C.; Scheutjens, J. M. H. M.; Cosgrove, T.; Vincent, B. *Polymers at Interfaces*; Springer Netherlands: Dordrecht, 1998.

(38) Klein Wolterink, J.; van Male, J.; Cohen Stuart, M. A.; Koopal, L. K.; Zhulina, E. B.; Borisov, O. V. Annealed Star-Branched Polyelectrolytes in Solution. *Macromolecules* **2002**, *35*, 9176–9190.

(39) Li, Z.; Kesselman, E.; Talmon, Y.; Hillmyer, M. A.; Lodge, T. P. Multicompartment Micelles from ABC Miktoarm Stars in Water. *Science* **2004**, *306*, 98–101.

(40) Sun, G.; Cui, H.; Lin, L. Y.; Lee, N. S.; Yang, C.; Neumann, W. L.; Freskos, J. N.; Shieh, J. J.; Dorshow, R. B.; Wooley, K. L. Multicompartment Polymer Nanostructures

with Ratiometric Dual-Emission pH-Sensitivity. *Journal of the American Chemical Society* **2011**, *133*, 8534–8543, PMID: 21574617.

(41) Shi, P.; Gao, C.; He, X.; Sun, P.; Zhang, W. Multicompartment Nanoparticles of Poly(4-vinylpyridine) Graft Block Terpolymer: Synthesis and Application as Scaffold for Efficient Au Nanocatalyst. *Macromolecules* **2015**, *48*, 1380–1389.

(42) Meristoudi, A.; Pispas, S.; Vainos, N. Self-assembly in solutions of block and random copolymers during metal nanoparticle formation. *Journal of Polymer Science Part B: Polymer Physics* **2008**, *46*, 1515–1524.

(43) Provencher, S. W. CONTIN: A general purpose constrained regularization program for inverting noisy linear algebraic and integral equations. *Computer Physics Communications* **1982**, *27*, 229–242.

(44) Radulescu, A. et al. Tuning the instrument resolution using chopper and time of flight at the small-angle neutron scattering diffractometer KWS-2. *Journal of Applied Crystallography* **2015**, *48*, 1849–1859.

(45) Hansen, C. M. *Hansen Solubility Parameters*; CRC Press, 2007.

Graphical TOC Entry